Mahan excitons in degenerate wurtzite InN: Photoluminescence spectroscopy and reflectivity measurements

Martin Feneberg,* Jürgen Däubler, Klaus Thonke, and Rolf Sauer
Institut für Halbleiterphysik, Universität Ulm, 89069 Ulm, Germany

Pascal Schley and Rüdiger Goldhahn
Institut für Physik, Technische Universität Ilmenau, PF 100565, 98684 Ilmenau, Germany

(Received 11 February 2008; revised manuscript received 23 April 2008; published 17 June 2008)

Unintentionally degenerately doped *n*-type hexagonal wurtzite InN samples were studied by using Fourier-transform photoluminescence spectroscopy and reflectivity measurements. We found in luminescence overlapping band acceptor (e,A^0) transitions related to two different acceptors with a strong enhancement of their intensities close to the Fermi energy of the electrons recombining with the localized holes. Our explanation is in terms of a Fermi-edge singularity of the electrons due to strongly increased electron-hole scattering. Electron-hole pairs with such resonantly enhanced oscillator strengths have been referred to as Mahan excitons. Temperature-dependent reflectivity measurements confirm this interpretation.

DOI: 10.1103/PhysRevB.77.245207 PACS number(s): 71.10.Ca, 78.55.Cr, 71.35.−y

I. INTRODUCTION

The increased availability of high-quality wurtzite InN has recently triggered much research on this technologically interesting material. Many basic problems of the material are now well understood whereas others have remained vague. The most fundamental parameter of a semiconductor is the band gap energy, which in the case of InN has been controversially discussed. Early research had yielded a band gap of about 1.9 eV in polycrystalline InN samples.[1,2] Based on investigations of single-crystalline layers, this value was later corrected to be much lower, amounting to only ≈ 0.7 eV.[3] This value was, in turn, recently called into question, suggesting that the observed infrared luminescence band underlying the interpretation was not due to a band-to-band transition, as supposed, but rather to metallic indium clusters. Instead, a new value of 1.4 eV was postulated[4] but was also not widely accepted in the community.[5] A very recent study of spectroscopic ellipsometry and photoreflectivity finds the zero-density band gap to be $E_g=0.68$ eV at room temperature.[6] We feel that many of the problems in interpreting the luminescence spectra of InN can be traced back to the fact that either a very high-doped $(n>10^{19}\ \mathrm{cm}^{-3})$ material was investigated or—even in the case of lower doping $(n<10^{18}\ \mathrm{cm}^{-3})$—the samples were still degenerate.

In the present study, we report detailed photoluminescence (PL) and reflectivity experiments on single-crystalline InN epitaxial layers with intermediate carrier concentrations $(10^{18}\ \mathrm{cm}^{-3}<n<10^{19}\ \mathrm{cm}^{-3})$. In this range of electron densities, the samples are still degenerate but the Burstein-Moss shift, owing to the conduction band filling, begins to overcompensate the band gap renormalization due to the electron exchange interaction.

II. EXPERIMENT

The InN layers used in this study were all grown by molecular beam epitaxy on sapphire substrates with nucleation and thin intermediate layers. Sample 1 was grown at Cornell University, Ithaca, New York.[7] The InN layer is about 500 nm thick and has an In-polar surface. Samples 2 and 3 were grown at Chiba University, Japan.[8] They are both about 2.3 μm thick and have N-polar surface. The lattice constants of all samples were determined by x-ray diffraction measurements. The in-plane lattice constants of $a=3.5280$, 3.5302, and 3.5295 Å were obtained for samples 1, 2, and 3, respectively. These values are lower than the strain-free value of $a=3.5377$ Å.[9] The in-plane strain of all samples was also confirmed by Raman measurements. The in-plane compressive strain of $\varepsilon_{xx}\approx -2.7\times 10^{-3}$ (sample 1), -2.1×10^{-3} (sample 2), and -2.3×10^{-3} (sample 3) causes a blueshift[10,11] of the band gap energy of 15 (sample 1), 11 (sample 2), and 12 meV (sample 3), in comparison to strain-free material ($E_g=0.68$ eV at room temperature). PL studies for differently strained films with similar carrier densities confirm the band gap shifts.[12] Hall measurements revealed carrier concentrations of $n=1\times 10^{18}$, 3.5×10^{18}, and $3.4\times 10^{18}\ \mathrm{cm}^{-3}$ for samples 1, 2, and 3, respectively. Due to the surface accumulation layer, the carrier density in the bulk of the samples is lower than the value determined by the Hall measurements.[10,13,14] Therefore, infrared spectroscopic ellipsometry (IR-SE) studies were carried out to determine the plasma frequency (ω_p) from which the bulk electron concentration is obtained by a self-consistent analysis of the effective mass change related with the band gap renormalization.[15] The transition energy at the Fermi edge at room temperature results from fitting the dielectric function in the energy region around the gap by a method described in detail in Ref. 6. For the PL measurements, the samples were mounted in a variable-temperature liquid-helium bath cryostat and excited by the 514.5 nm line of an Ar^+ laser with a typical power of 100 mW. The collected light was analyzed by a Fourier-transform spectrometer Bomem DA8 with a liquid-nitrogen cooled InAs diode having a cutoff wavelength of 3.12 μm. The reflectivity measurements were carried out in the same setup. A quartz-halogen lamp was used as a broadband light source while a gold-coated silicon wafer served as a reference mirror.

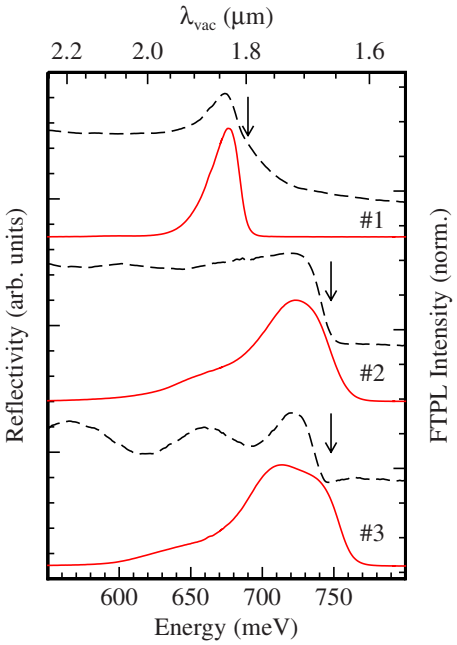

FIG. 1. (Color online) Low-temperature (4.2 K) photoluminescence (full line) and reflectivity (dashed line) spectra, showing the near band gap region. The arrows mark the position of the Fermi energy.

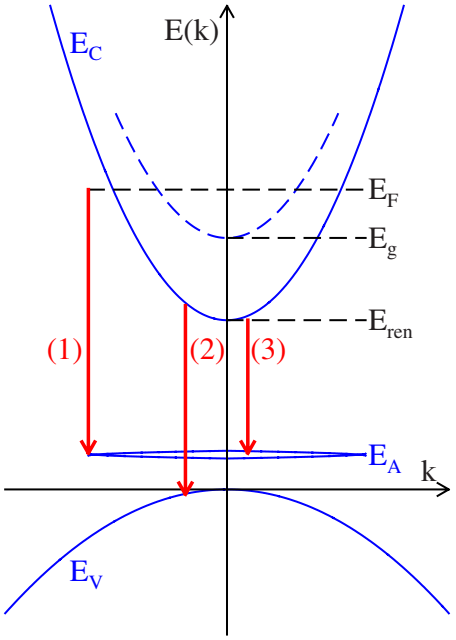

FIG. 2. (Color online) Schematic of the optical transitions in the degenerate InN: (1) Recombination of an electron close to the Fermi edge E_F with a hole localized at an acceptor with an enhanced transition probability due to the Fermi-edge singularity (Mahan exciton), (2) band-to-band transition at low k, and (3) band-to-acceptor transition.

III. RESULTS AND DISCUSSION

The low-temperature PL spectra of all three samples are exhibited in Fig. 1 together with their corresponding reflectivity measurements. All of the samples show a strong luminescence signal in the infrared region between 600 and 750 meV photon energy with no further luminescence at higher energies up to the photon energy of the exciting laser beam (2.41 eV). The (low-temperature) Fermi energy E_F was determined by the reflectivity spectra. Due to the conduction band filling, the absorption and reflectivity edges are located at higher energies than the renormalized band edge E_{ren}, which is, in turn, downshifted from E_g due to the exchange interaction of the electrons in the high-density electron plasma. The low-temperature Fermi energies are obtained from the reflectivity onsets in the spectra. In our case, the values are $E_F=(0.69\pm0.02)$ eV (sample 1) and (0.75 ± 0.01) eV (samples 2 and 3) with experimental uncertainties due to the broadening of the reflectivity edges.

In PL, sample 1 shows a single transition peaking at 0.676 eV with a line shape typical for degenerate doping: The low-energy edge of the spectrum is determined by the combined density of states washed out by the conduction band tail arising from the high doping and the high-energy edge is given by the sharp cutoff of the Fermi occupation function convolved with a Lorentzian determined by lifetime broadening.

Equivalent spectra, showing the same trend for different carrier densities, were recently observed in similarly or lower doped samples.[11,16–18] Based on the line-shape analysis, they were explained as being due to the conduction band-to-acceptor transitions involving shallow acceptors with binding energies between 5–18 and 50–85 meV. In the following sections, we will also perform line-shape analyses and show that the luminescence in our samples is also due to electron-acceptor (e,A^0) transitions, however, in our case resonantly enhanced at the electron Fermi edges. To simplify this discussion, we plot in Fig. 2 three relevant optical transitions: (1) electrons at the Fermi edge in the degenerate plasma recombine with localized holes at acceptors while the k spread of the acceptor hole wave function allows for transitions up to high k values; (2) electron-hole recombination between the bands obeying the k conservation and, thus, being possible only with low k values since no excited hole states are occupied; and (3) low-energy transitions from the electron states close to the renormalized gap E_{ren} to acceptor-bound holes.

In Fig. 3, the temperature dependence of the single transition of sample 1 is displayed shifting from 0.676 eV (peak position) at 10 K to 0.647 eV at 290 K. Also, the high-energy edge is significantly washed out, reflecting the softening of the Fermi function at room temperature. Assuming that the transition is due to an (e,A^0) recombination process, we are concerned with a line shape of the form

$$I(\hbar\omega)\sim\sqrt{\hbar\omega-(E_{\mathrm{ren}}-E_A)}\left(1+\exp\frac{\hbar\omega-E_F^e}{k_bT}\right)^{-1}. \quad (1)$$

Owing to the degeneracy of the sample, the Fermi probability function enters Eq. (1), where E_F^e is the electron Fermi level in the initial quasiequilibrium state of the transition and $E_F^e\approx E_F$ in thermal equilibrium, as the photocreated excess electron density is small compared to the doping density. In the spectra of sample 1, a second spectral component is

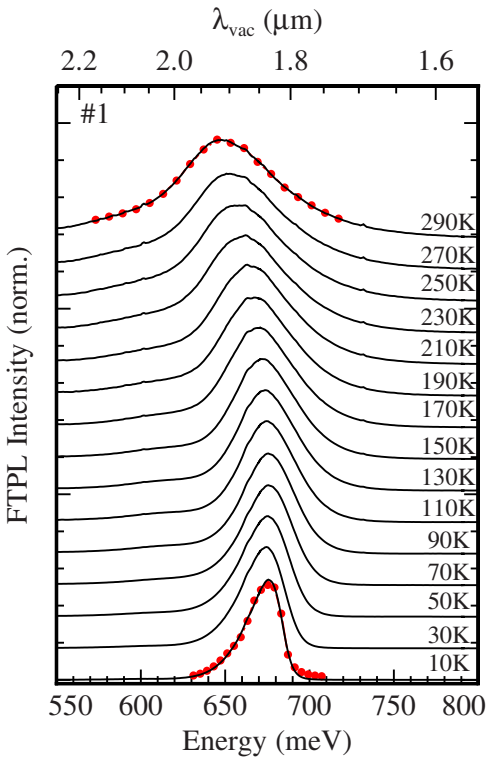

FIG. 3. (Color online) Normalized photoluminescence spectra of sample 1 as a function of temperature. The spectra are vertically shifted for clarity. For 10 and 290 K, the line-shape fits are exemplarily shown.

weakly visible ≈72 meV below the main transition due to the coupling of LO phonons. This satellite was taken into account modeling it by a band of the form of Eq. (1) shifted by the LO-phonon energy and having a temperature-dependent intensity. It is found that the tail of the conduction band can be well modeled by a Gaussian distribution with a width of 15 meV due to the high doping concentration. Finally, $I(\hbar\omega)$ was convolved with a Lorentzian accounting for lifetime broadening. The fits to the experimental spectra are exemplarily shown in Fig. 3 for 10 and 290 K. The thermally induced band gap shrinkage was taken into account by the expression given by Viña *et al.*[19] in the form

$$E_{\mathrm{ren}}(T) = E_{\mathrm{ren}}(0) - E_A - \frac{\alpha\Theta}{\exp\Theta/T - 1}. \qquad (2)$$

We extracted the parameters $E_{\mathrm{ren}}(T=0)-E_A=0.654$ eV, $\Theta=681$ K, and $\alpha=0.4$ meV/K from the fits. At room temperature, we find $E_{\mathrm{ren}}(RT)-E_A=0.622$ eV. If we use the room-temperature band gap energy $E_g=695$ meV, as determined by spectral ellipsometry, we can calculate the sum of the acceptor ionization energy E_A and the band gap renormalization energy, amounting to 695 meV−622 meV =73 meV. Because the band gap renormalization E_g-E_{ren} =44 meV is known from model calculations,[6] we obtained an acceptor ionization energy of $E_A=29$ meV in sample 1. The thermal variation of the band gap energy amounts to $\Delta E_g(0\rightarrow 290\ \mathrm{K})=32$ meV, being in agreement with the value of ≈33 meV reported in Ref. 20. This line-shape analysis confirms our earlier assumption that the PL spectrum of sample 1 is due to (e,A^0) recombination. A summary of the energy values of all three samples is given in Table I.

TABLE I. Summary of characteristic values of the investigated samples. The energy values are all in meV. ω_p is the plasma frequency with values expressed as wave numbers and n_H (n_{opt}) is the carrier density determined by Hall measurements (IR-SE). The low-temperature energy values are determined by PL, 300 K values by IR-SE and corresponding calculations. The theoretical curves in Fig. 7 are consistent with these values within reasonable error.

Sample	1	2	3
n_H (10^{18} cm^{-3})	1.0	3.5	3.4
μ (cm^2 V^{-1} s^{-1})	1000	1380	1450
$\bar{\omega}_p/(2\pi)$ (cm^{-1})	362	705	692
n_{opt} (10^{18} cm^{-3})	0.8	3.1	3.0
E_g (290 K)	695	691	692
E_{ren} (290 K)	651	618	619
E_F (290 K)	682	725	724
E_{ren} (10 K)	683	650	651
E_F (10 K)	690	750	750

Our higher doped samples 2 and 3 show more complicated PL spectra. At first sight, there seem to be two different contributions to the spectra in Fig. 1: a weak low-energy band extending down to ≈600 meV photon energy and a much stronger overlapping band with a maximum in the range of 730 meV. For sample 3, this latter band itself obviously consists of two components. The temperature-dependent PL measurements (Figs. 4 and 5) demonstrate that the high-energy band has indeed two closely spaced components in both samples. Our analysis below shows that for either sample the whole spectrum is undividedly a band-to-acceptor transition whose intensity is strongly enhanced at the Fermi-energy edge of the electrons and where the two close-lying high-energy components arise from the participation of two different acceptors.

A quantitative line-shape analysis similar to that of sample 1 is not possible for samples 2 and 3 due to the strong intensity enhancement at ≈730 meV (10 K) far above the low-temperature band edge. Observing the following qualitative features, we assign the PL spectra to (e,A^0) transitions: In both samples (Figs. 4 and 5), the weak low-energy component with a maximum at around 650 meV (10 K) monotonically shifts to lower energies with increasing sample temperature. Furthermore, a phonon replica at ≈72 meV lower energy shows up for $T\geq 150$ K shifting with it. The strong transition at the Fermi energy at around 720 meV (10–70 K) shows an *S*-shaped energy shift with increasing temperature and becomes successively weaker relative to the low-energy portion of the band-acceptor spectrum. Also, the above mentioned second high-energy component is fairly well observable at ≈30–40 meV higher energy.

The energy spacing of the two high-energy components of ≈35 meV is consistent with the energy difference of the two acceptor states in Refs. 16 and 18, corroborating our spec-

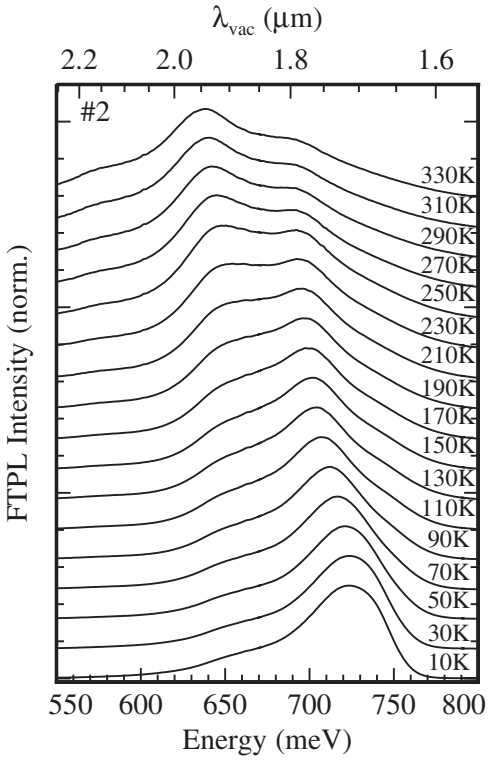

FIG. 4. Normalized photoluminescence spectra of sample 2 as a function of temperature. The spectra are vertically shifted for clarity.

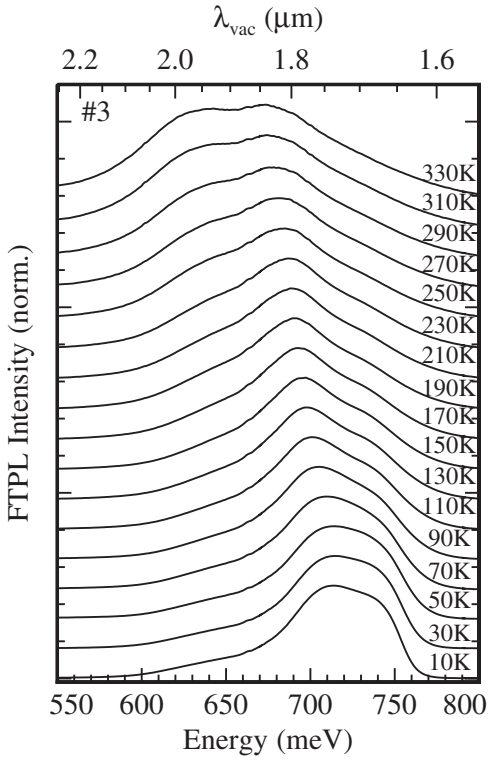

FIG. 5. Normalized photoluminescence spectra of sample 3 as a function of temperature. The spectra are vertically shifted for clarity.

trum interpretation of samples 2 and 3 in terms of two different but overlapping (e,A^0) transitions. However, we cannot exclude the possibility that these two high-energy bands are due to a Mahan exciton bound to the same acceptor found in sample 1 ($E_A=29$ meV) and to a Mahan exciton consisting of an electron at the Fermi edge directly recombining with a free hole from the valence band. The energy spacing of ≈ 35 meV would be consistent with this alternative interpretation, which we nonetheless consider to be less probable since the occupation probability of holes at the Fermi edge is vanishingly low while the intensity of this band at higher temperatures is still significant. In either case, the spectral enhancement of the luminescence band far above the band gap cannot be explained by conventional band-to-acceptor or by band-to-band transitions.

We interpret the high-energy components of the spectrum in terms of "Mahan excitons."[21] A Mahan exciton can be thought of as a localized hole interacting with all the electrons in the whole electron Fermi sea. The exclusion principle suppresses multiple electron-hole scattering processes as long as the electron energy is smaller than E_F^e and, consequentially, only a weak, broad (e,A^0) spectrum is emitted [transition (3) in Fig. 2]. At the Fermi edge, the scattering rates are strongly enhanced, leading to a singularity and concomitantly strong enhancement of the optical matrix element. The hole of the Mahan exciton needs to be localized to provide a sufficiently large spread in k space so that k-preserving transitions from the high-energy (and high-k) electron states are possible [transition (1) in Fig. 2]. A band-to-band Mahan exciton transition is basically also possible but should be much weaker in intensity due to the vanishingly small number of holes in the valence band at the Fermi vector k_F. The band-to-band transition at $k \approx 0$ [transition (2) in Fig. 2] should be even weaker, presumably by the same factor as the Mahan exciton compared to the (e,A^0) band. The electric dipole transitions of the Mahan exciton at the Fermi edge should show resonant behavior in its emission, absorption, and reflectivity. A Fermi-edge singularity was first observed in the luminescence of a two-dimensional electron gas in InGaAs-InP by Skolnick *et al.*[22] Later, it was also found in bulk semiconductors apparently for the first time in InAs by Fuchs *et al.*[23]

The interpretation of our spectra as being due to Mahan exciton recombination is strongly supported by the observed "thermalization" behavior of the Fermi-edge singularity. The strength of the optical matrix element at the Fermi energy critically depends on the sharpness of the Fermi edge being smeared out at increasing temperature.[24] The reflectivity spectra of sample 1 in Fig. 6 show the expected resonant enhancement of the signal at the Fermi edge at low temperatures, which goes over into the usual reflectivity step at increasing temperatures. The resonance with a maximum position at 673 meV (4.2 K) has its characteristic energy at the Fermi energy of $E_F=(0.69\pm0.02)$ eV. The model calculations[6] predict a low-temperature Fermi edge of 714 meV for the same sample, which is in reasonable agreement with the value observed.

Experimentally, the observation of the reflectivity resonance and its disappearance in Fig. 6 was possible since sample 1 is wedge shaped, preventing Fabry-Pérot oscilla-

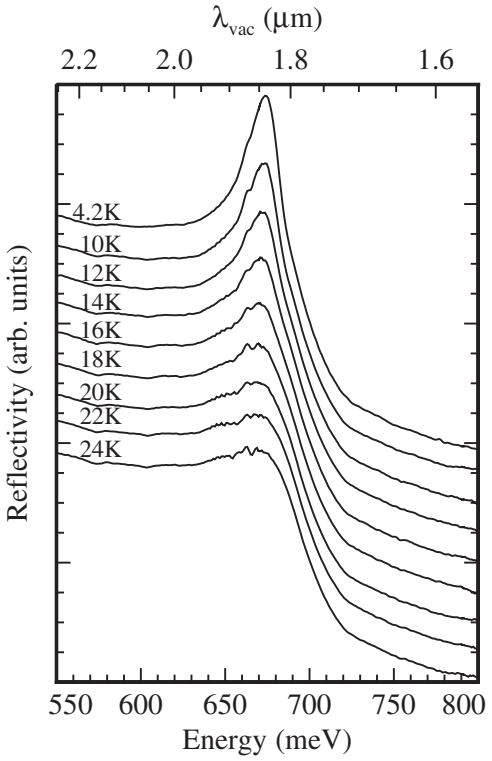

FIG. 6. Reflectivity spectra of sample 1 for temperatures between 4.2 and 24 K showing thermalization of the resonance below the Fermi energy.

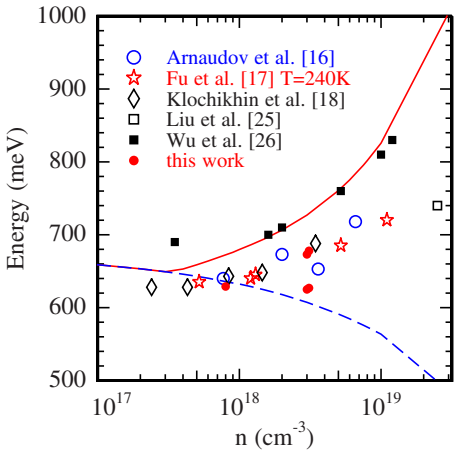

FIG. 7. (Color online) Calculated dependence of the renormalized band gap energy (dashed line) and the Fermi energy (full line) on the carrier density in degenerately doped *n*-type InN at room temperature and its comparison to the experimental data. Full squares represent room-temperature absorption data taken from Ref. 26. Other symbols refer to the photoluminescence peak positions of samples 1–3, which were corrected for the strain shifts, and to additional data taken from the literature, as indicated. The data from low-temperature PL are shifted by 32 meV due to the temperature-dependent band gap shrinkage.

tions, as seen in the reflectivity spectra of samples 2 and 3. We expect the Mahan excitons to play a role in many of the optical data published on moderately degenerate InN samples although they were not explicitly discussed in the corresponding analysis of the data. The unusual line shapes of the low-temperature PL spectra in Refs. 12, 17, and 25, for example, might hint to the participation of Mahan excitons.

In Fig. 7, literature data of room-temperature PL peak energies and absorption edges[26] versus the carrier densities are displayed. For comparison, calculated energies of the renormalized band gap and the Burstein-Moss shift as a function of carrier density are shown. The band gap renormalization due to the electron-electron exchange and electron–donor core interactions were calculated by the approach presented in Ref. 27. The effective electron mass in the renormalization terms was taken as an average of the masses over the occupied conduction band states. The energy-dependent masses of the electrons filling the conduction band states from the renormalized gap up to E_F were calculated from the dispersion relation obtained from **kp**-perturbation theory, taking the threefold valence band into account. As in a previous work,[6] we used in the correction term $2\langle P\rangle^2/(E_{\mathrm{ren}}m_0)$ to the reciprocal electron mass a value of $\langle P\rangle^2/m_0=10$ eV. Owing to the energy-dependent electron mass, the renormalization only roughly follows a $n^{1/3}$ dependence while the band filling proceeds with a Fermi energy approximately proportional to $n^{2/3}$. Adding these two energy correction terms to the strain-free fundamental zero density energy gap, $E_g=0.68$ eV at room temperature,[6] we obtain the transition energy at the Fermi edge as a function of the electron concentration. At increasing electron densities, a band-to-acceptor or a band-to-band transition should mirror the energy shift of the renormalized gap at the low-energy onset of the luminescence. In contrast, a Mahan exciton should spectroscopically slowly approach the Fermi energy since its binding energy goes to zero for high electron densities.[21,24] The localized holes are needed for a Mahan exciton to exist; hence, we expect the transition energy of the Mahan exciton in InN to be lower than the Fermi edge by the amount of the acceptor ionization energy and the (very small) binding energy of the Mahan exciton. It was already mentioned that Arnaudov and co-workers[16] have identified at least two optically active acceptor states in a relatively low-doped InN. Our data also give clear evidence for two acceptors in samples 2 and 3 being responsible for the two overlapping high-energy peaks in the 700–750 meV spectral region and enabling Mahan exciton recombination at these two acceptors.

IV. CONCLUSION

In conclusion, we have consistently explained the luminescence spectra in our wurtzite InN samples as governed by Mahan excitons. The interpretation was based on PL and reflectivity measurements with further data necessary for the discussion coming from spectroscopic ellipsometry. An incomplete review of literature data shows that the PL peak energy positions are shifted in agreement with the band gap renormalization and band filling, suggesting that in these cases also, the peaks are due to the recombination of Mahan excitons.

ACKNOWLEDGMENTS

We thank W. J. Schaff (Department of Electrical and Computer Engineering, Cornell University, USA) and A. Yoshikawa (Department of Electronics and Mechanical Engineering, Chiba University, Japan) for the samples. We also acknowledge the assistance of G. M. Prinz (Institut für Halbleiterphysik, Universität Ulm, Germany) in the Raman measurements, and of S. Schwaiger (Institut für Halbleiterphysik, Universität Ulm, Germany) and V. Cimalla (now at Fraunhofer Institute for Applied Solid-State Physics, Germany) in the x-ray analysis.

*martin.feneberg@uni-ulm.de

[1] K. Osamura, K. Nakajima, Y. Murakami, P. H. Shingu, and A. Ohtsuki, Solid State Commun. **11**, 617 (1972).
[2] T. L. Tansley and C. P. Foley, J. Appl. Phys. **59**, 3241 (1986).
[3] V. Y. Davydov, A. A. Klochikhin, R. P. Seisyan, V. V. Emtsev, S. V. Ivanov, F. Bechstedt, J. Furthmüller, H. Harima, A. V. Mudryi, J. Aderhold, O. Semchinova, and J. Graul, Phys. Status Solidi B **229**, R1 (2002).
[4] T. V. Shubina, S. V. Ivanov, V. N. Jmerik, D. D. Solnyshkov, V. A. Vekshin, P. S. Kop'ev, A. Vasson, J. Leymarie, A. Kavokin, H. Amano, K. Shimono, A. Kasic, and B. Monemar, Phys. Rev. Lett. **92**, 117407 (2004).
[5] F. Bechstedt, J. Furthmüller, O. Ambacher, and R. Goldhahn, Phys. Rev. Lett. **93**, 269701 (2004).
[6] P. Schley, R. Goldhahn, A. T. Winzer, G. Gobsch, V. Cimalla, O. Ambacher, H. Lu, W. J. Schaff, M. Kurouchi, Y. Nanishi, M. Rakel, C. Cobet, and N. Esser, Phys. Rev. B **75**, 205204 (2007).
[7] H. Lu, W. J. Schaff, J. Hwang, H. Wu, G. Koley, and L. F. Eastman, Appl. Phys. Lett. **79**, 1489 (2001).
[8] K. Xu and A. Yoshikawa, Appl. Phys. Lett. **83**, 251 (2003).
[9] W. Paszkowicz, R. Černý, and S. Krukowski, Powder Diffr. **18**, 114 (2003).
[10] C. S. Gallinat, G. Koblmüller, J. S. Brown, S. Bernardis, J. S. Speck, G. D. Chern, E. D. Readinger, H. Shen, and M. Wraback, Appl. Phys. Lett. **89**, 032109 (2006).
[11] A. Kamińska, G. Franssen, T. Suski, I. Gorczyca, N. E. Christensen, A. Svane, A. Suchocki, H. Lu, W. J. Schaff, E. Dimakis, and A. Georgakilas, Phys. Rev. B **76**, 075203 (2007).
[12] X. Wang, S. Che, Y. Ishitani, and A. Yoshikawa, J. Appl. Phys. **99**, 073512 (2006).
[13] V. Cimalla, V. Lebedev, F. M. Morales, R. Goldhahn, and O. Ambacher, Appl. Phys. Lett. **89**, 172109 (2006).
[14] P. D. C. King, T. D. Veal, and C. F. McConville, Phys. Rev. B **77**, 125305 (2008).
[15] P. Schley, R. Goldhahn, C. Napierala, G. Gobsch, J. Schörmann, D. J. As, K. Lischka, M. Feneberg, and K. Thonke, Semicond. Sci. Technol. **23**, 055001 (2008).
[16] B. Arnaudov, T. Paskova, P. P. Paskov, B. Magnusson, E. Valcheva, B. Monemar, H. Lu, W. J. Schaff, H. Amano, and I. Akasaki, Phys. Rev. B **69**, 115216 (2004).
[17] S. P. Fu, T. T. Chen, and Y. F. Chen, Semicond. Sci. Technol. **21**, 244 (2006).
[18] A. A. Klochikhin, V. Y. Davydov, V. V. Emtsev, A. V. Sakharov, V. A. Kapitonov, B. A. Andreev, H. Lu, and W. J. Schaff, Phys. Rev. B **71**, 195207 (2005).
[19] L. Viña, S. Logothetidis, and M. Cardona, Phys. Rev. B **30**, 1979 (1984).
[20] D. Y. Song, M. E. Holtz, A. Chandolu, A. Bernussi, S. A. Nikishin, M. W. Holtz, and I. Gherasoiu, Appl. Phys. Lett. **92**, 121913 (2008).
[21] G. D. Mahan, Phys. Rev. **153**, 882 (1967).
[22] M. S. Skolnick, J. M. Rorison, K. J. Nash, D. J. Mowbray, P. R. Tapster, S. J. Bass, and A. D. Pitt, Phys. Rev. Lett. **58**, 2130 (1987).
[23] F. Fuchs, K. Kheng, P. Koidl, and K. Schwarz, Phys. Rev. B **48**, 7884 (1993).
[24] S. Schmitt-Rink, C. Ell, and H. Haug, Phys. Rev. B **33**, 1183 (1986).
[25] B. Liu, R. Zhang, Z. L. Xie, X. Q. Xiu, Z. X. Bi, S. L. Gu, Y. Shi, Y. D. Zheng, L. J. Hu, Y. H. Chen, and Z. G. Wang, Appl. Phys. Lett. **87**, 176101 (2005).
[26] J. Wu, W. Walukiewiecz, S. X. Li, R. Armitage, J. C. Ho, E. R. Weber, E. E. Haller, H. Lu, W. J. Schaff, A. Barcz, and R. Jakiela, Appl. Phys. Lett. **84**, 2805 (2004).
[27] J. Wu, W. Walukiewicz, W. Shan, K. M. Yu, J. W. Ager III, E. E. Haller, H. Lu, and W. J. Schaff, Phys. Rev. B **66**, 201403(R) (2002).